Topological currents in black phosphorus with broken inversion symmetry

Tony Low,[1] Yongjin Jiang,[1,2] and Francisco Guinea[3,4]

[1]*Department of Electrical and Computer Engineering, University of Minnesota, Minneapolis, Minnesota 55455, USA*

[2]*Center for Statistical and Theoretical Condensed Matter Physics, ZheJiang Normal University, Jinhua 321004, Peoples Republic of China*

[3]*School of Physics and Astronomy, University of Manchester, Oxford Road, Manchester M13 9PL, England, United Kingdom*

[4]*IMDEA Nanociencia, Faraday 3, 28049 Madrid, Spain*

(Received 29 July 2015; published 30 December 2015)

We examine the nature of topological currents in black phosphorus when its inversion symmetry is deliberately broken. Here, the conduction- and valence-band edges are located at the Γ point of the rectangular Brillouin zone, and they exhibit strong anisotropy along its two crystal axes. We will show below that these salient features lead to linear transverse neutral topological currents, accompanied also by nonlinear transverse charge currents at the Fermi surface. These topological currents are maximal when the in-plane electric field is applied along the zigzag crystal axes but zero along the armchair direction.

DOI: 10.1103/PhysRevB.92.235447 PACS number(s): 73.21.−b, 73.22.Lp, 73.61.−r, 74.78.Fk

Topological current is a well-known physical manifestation when a crystalline solid possesses a finite Berry curvature [1–3]. The Berry curvature is a geometrical property of the Bloch energy band and acts as an effective magnetic field in momentum space [1]. Hence, topological materials may exhibit anomalous Hall-like transverse currents in the presence of an applied electric field, in the absence of a magnetic field. In topological insulators [4], topological bands with nontrivial Berry phase lead to propagating surface states that are protected against backscattering from disorder and impurities. In transition-metal dichalcogenides, the two valleys carry opposite Berry curvature, or magnetic moment, giving rise to bulk topological charge neutral valley currents [5–7]. Recently, these bulk topological currents were also experimentally investigated in other Dirac materials, such as gapped graphene and bilayer graphene systems [8,9].

In this paper, we will show that black phosphorus (BP) belongs to a broad class of insulating systems with a nontrivial band structure, where a finite Berry curvature in patches of the Brillouin zone leads to dissipationless edge currents [7]. Unlike topological insulators [4], the system we are concerned with in this paper has a zero integrated Berry curvature over a given band, so that there are no edge states. Nevertheless, the system that we study has a nonzero Berry curvature over finite regions of the Brillouin zone, where regions with opposite Berry curvature are contiguous, and near the center of the Brillouin zone. They lead to the existence of topological edge currents, which does not require edge states within the insulating gap and behaves differently from topological currents in more well-studied systems such as gapped graphene and transition-metal dichalcogenides [5–7].

Below, we examine the nature of these topological currents in BP [10–12], when its inversion symmetry is deliberately broken. Unlike more well-studied two-dimensional (2D) materials such as graphene and transition-metal dichalcogenides, several key differences are notable. First, in monolayer BP, the conduction- and valence-band edges are located at the Γ point of the rectangular Brillouin zone [13]. Second, the energy bands exhibit strong anisotropy along its two crystal axes. We will show below that these salient features will lead to linear transverse *neutral* topological currents, accompanied also by a nonlinear transverse *charge* current. These topological currents are maximal (zero) when the in-plane electric field is applied along the zigzag (armchair) crystal axes. We discuss how these topological effects can be detected electrically and optically.

In this work, we consider monolayer BP, described with a four-band tight-binding model [13] as illustrated in Fig. 1(a). We construct Bloch-like basis functions $|\chi_j^{\mathbf{k}}\rangle = \sum_{\mathbf{R}} \exp[i\mathbf{k}\cdot(\mathbf{R}+\mathbf{b}_j)]|\phi_j^{\mathbf{R}}\rangle$ where $\mathbf{R}$ and $\mathbf{b}_j$ are the lattice and basis vectors, and the index j runs over all the phosphorus atoms within the primitive cell, with a single orbital on each atom denoted by $|\phi_j^{\mathbf{R}}\rangle$. The Hamiltonian matrix can then be constructed from

$$\mathcal{H}_{ij}(\mathbf{k}) = \langle\chi_j^{\mathbf{k}}|\mathcal{H}|\chi_j^{\mathbf{k}}\rangle = \sum_{\mathbf{R}} e^{i\mathbf{k}\cdot(\mathbf{R}+\mathbf{b}_j-\mathbf{b}_i)}h_{ij} \tag{1}$$

where $h_{ij} \equiv \langle\phi_i^{\mathbf{0}}|\mathcal{H}|\phi_j^{\mathbf{R}}\rangle$ contains the tight-binding hopping parameter. The hopping parameters [13] used in this work are $t_1 = -1.22\,\text{eV}$, $t_2 = 3.67\,\text{eV}$, $t_3 = -0.205\,\text{eV}$, $t_4 = -0.105\,\text{eV}$, and $t_5 = -0.055\,\text{eV}$. The secular equation to be solved is $\mathcal{H}_{\mathbf{k}}|\Psi_{n\mathbf{k}}\rangle = E_{n\mathbf{k}}|\Psi_{n\mathbf{k}}\rangle$, where $\mathcal{H}_{\mathbf{k}}$ is the 4×4 matrix of elements $\mathcal{H}_{ij}(\mathbf{k})$, $|\Psi_{n\mathbf{k}}\rangle$ and $E_{n\mathbf{k}}$ are the eigenvectors and eigenenergies.

The Berry curvature for the electronic Bloch states of the nth band can then be computed from [2]

$$\Omega_n(\mathbf{k}) = \Omega_n(\mathbf{k})\hat{\mathbf{z}} = \nabla_{\mathbf{k}} \times \langle\Psi_{n\mathbf{k}}|i\nabla_{\mathbf{k}}|\Psi_{n\mathbf{k}}\rangle \tag{2}$$

and its magnitude has the following explicit form:

$$\Omega_n(\mathbf{k}) = 2\Im\left[\sum_{m\neq n} \frac{\langle\Psi_{n\mathbf{k}}|i\partial_{k_x}|\Psi_{m\mathbf{k}}\rangle\langle\Psi_{m\mathbf{k}}|i\partial_{k_y}|\Psi_{n\mathbf{k}}\rangle}{(E_{m\mathbf{k}}-E_{n\mathbf{k}})^2}\right]. \tag{3}$$

Time-reversal symmetry implies that $\Omega_n(\mathbf{k}) = -\Omega_n(-\mathbf{k})$, while a crystal lattice with inversion symmetry would require $\Omega_n(\mathbf{k}) = \Omega_n(-\mathbf{k}) = 0$. Hence, inversion symmetry breaking is necessary to generate a finite Berry curvature.

We consider some basic symmetry properties of the Hamiltonian. When the on-site potentials V_j are zero, there are two inversion centers, i.e., between atom 1 and 2 and between atom 2 and 3. We denote these space inversion symmetries as $\mathcal{P}_1$ and $\mathcal{P}_2$, respectively. In addition, we have mirror-symmetry operations $\mathcal{M}_x$, which interchange atoms 1 and 2 with atoms 4 and 3, respectively, and $\mathcal{M}_y$, which is

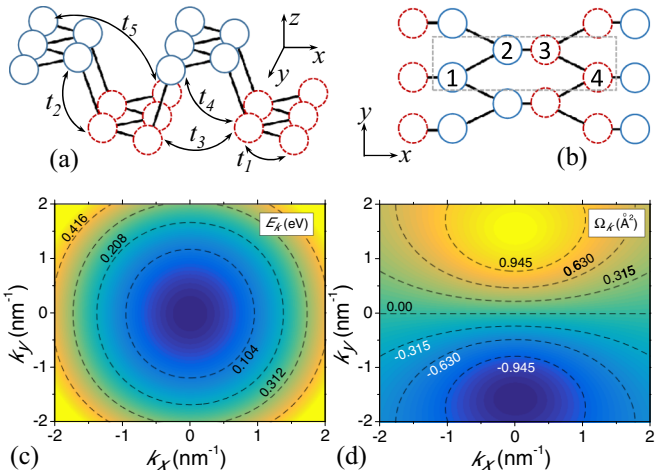

FIG. 1. (Color online) (a) Crystal structure of monolayer black phosphorus and the hopping parameters included in the tight-binding model. Here, x is along the so-called armchair direction, while y is along the zigzag direction. (b) Top view of the crystal structure, and the primitive unit cell is also indicated. (c) and (d) Energy dispersion, $E_{\mathbf{k}}$, and its Berry curvature, $\Omega_{\mathbf{k}}$, for the conduction band in the vicinity of the band minimum at the Γ point. Inversion symmetry is broken by applying the following potentials to the basis atoms: $V_{1,4} = 0\,\mathrm{eV}$, $V_2 = -0.5\,\mathrm{eV}$, and $V_3 = 0.5\,\mathrm{eV}$.

diagonal in the atomic species space. We constrain ourselves to inversion symmetry-breaking schemes with only electrostatic on-site potentials V_j within each unit cell. First, consider a perpendicular electric field, i.e., $V_1 = V_2 \neq V_3 = V_4$; it breaks $\mathcal{M}_x$ and $\mathcal{P}_2$, but not $\mathcal{M}_y$ and $\mathcal{P}_1$. Second, consider electrostatic potentials staggering along the y (zigzag) direction, i.e., $V_2 = V_3 \neq V_1 = V_4$. This scheme breaks only $\mathcal{P}_1$, but not $\mathcal{P}_2$, $\mathcal{M}_x$, and $\mathcal{M}_y$. On the other hand, an electrostatic potential staggering along the x (armchair) direction will break all inversion symmetries and $\mathcal{M}_x$, except for $\mathcal{M}_y$. Although this configuration can generate nonzero Berry curvature, additional symmetries ensure zero transverse currents in this case, a subtle point on which we will elaborate below.

Alternatively, the combination of an out-of-plane electric field and an in-plane lattice commensurate electric field directed along the y direction can break all inversion symmetries, since $V_4 - V_3 = V_2 - V_1 \neq 0$. For example, let us consider $V_{1,4} = 0\,\mathrm{eV}$, $V_2 = -0.5\,\mathrm{eV}$, and $V_3 = 0.5\,\mathrm{eV}$. Figures 1(c) and 1(d) plot the energy dispersion, $E_{\mathbf{k}}$, and its Berry curvature, $\Omega_{\mathbf{k}}$, for the conduction band in the vicinity of the band minimum at the Γ point. The smaller electron effective mass along the armchair direction, x, leads to stronger dispersion as shown. Indeed, $\Omega_{\mathbf{k}}$ is finite and can take either sign in the Fermi sea of the Γ valley. This is reminiscent of the conventional valley physics, e.g., in gapped graphene and transition-metal dichalcogenides where the Berry curvatures of the two valleys bear opposite signs, except we have only a single valley in this case.

In the above-mentioned scheme, the mirror symmetry $\mathcal{M}_y$ is maintained, even when its inversion symmetries are being deliberately broken. Time-reversal symmetry requires that its energy dispersion respects $E_n(\mathbf{k}) = E_n(-\mathbf{k})$. The above-mentioned mirror symmetry would entail $E_n(k_x,k_y) = E_n(k_x,-k_y)$. These symmetries in combination also imply $E_n(k_x,k_y) = E_n(-k_x,k_y)$. For the Berry curvature, which is analogous to an effective magnetic field, to produce a physical observable that respects this $\mathcal{M}_y$ mirror symmetry would require $\Omega_n(k_y) = -\Omega_n(-k_y)$. Time-reversal symmetry would then impose the additional constraint that $\Omega_n(k_x) = \Omega_n(-k_x)$. This accounts for the form of the computed Berry curvature shown in Fig. 1(d).

Following these considerations, we examine the nature of topological currents arising from the induced Berry curvature, within the semiclassical Boltzmann transport theory. In the presence of an external electric field $\boldsymbol{\xi}$, the carrier velocity acquires a nonclassical transverse term due to Berry curvature as shown [2]:

$$\mathbf{v}_n(\mathbf{k}) = \frac{1}{\hbar}\nabla_{\mathbf{k}} E_{n\mathbf{k}} - \frac{e}{\hbar}\boldsymbol{\xi} \times \Omega_n(\mathbf{k}). \tag{4}$$

The transverse currents can be partitioned into contributions from the forward and backward propagating states, denoted by $\mathcal{J}^{\pm}$. By the former (latter), we refer to states the $\mathbf{v}_n(\mathbf{k})$ of which is such that $S \equiv \mathrm{sign}(\mathbf{v}_n \cdot \boldsymbol{\xi}) = \pm$, respectively. $\mathcal{J}^{\pm}$ can be computed semiclassically up to second order in the electric field, i.e., $\sigma^{\pm}_{\mathrm{bulk}}\xi + \sigma^{\pm}_{\mathrm{surf}}\xi^2 + O(\xi^3)$, with the conductivities defined as

$$\sigma^{\pm}_{\mathrm{bulk}} = -\frac{e}{\hbar}\int_{S=\pm} d\mathbf{k} f_0(\mathbf{k})\Omega(\mathbf{k}),$$
$$\sigma^{\pm}_{\mathrm{surf}} = \frac{e^2\tau}{\hbar^2}\int_{S=\pm} d\mathbf{k}[\nabla_{\mathbf{k}} f_0(\mathbf{k}) \cdot \boldsymbol{\xi}]\Omega(\mathbf{k}) \tag{5}$$

where $f_0(\mathbf{k})$ is the Fermi-Dirac distribution function, and τ is the electron scattering time. The linear contribution to $\mathcal{J}$ is a "bulk Fermi sea" phenomenon and can be partitioned into forward/backward propagating currents $\mathcal{J}^{\pm}_{\mathrm{bulk}}$ as illustrated in Fig. 2(a). These are counterpropagating currents which persist even when the system is in equilibrium. These transverse currents are certainly charge neutral since $\mathcal{J}^{+}_{\mathrm{bulk}} = -\mathcal{J}^{-}_{\mathrm{bulk}}$. Nevertheless, recent experiments have shown that such transport effects can be detected via a nonlocal transport measurement [8,9].

On the other hand, the nonlinear contribution to $\mathcal{J}$ is a "Fermi-surface" contribution, and can also be partitioned into $\mathcal{J}^{\pm}_{\mathrm{sur}}$ [see Fig. 2(b)]. These currents, however, are nonequilibrium in nature and require an electrochemical potential bias. For example, Fig. 2(c) illustrates the flows of the various current components in a typical two terminal device under bias. Unlike bulk currents, the latter has a net charge current since $\mathcal{J}^{+}_{\mathrm{sur}} = \mathcal{J}^{-}_{\mathrm{sur}}$. We contrast this with conventional valley physics where Fermi-surface contributions lead to transverse charge neutral currents instead, due to exact cancellation from the two valleys. Recent work found that finite nonlinear current can arise when the two valleys are not isotropic [14], leading to partial cancellation. In a single valley system like BP, the effect will be maximal.

The symmetry of the Berry curvature, i.e., $\Omega_n(k_y) = -\Omega_n(-k_y)$ and $\Omega_n(k_x) = \Omega_n(-k_x)$, has important consequences on the orientation dependence of the various transverse currents. $\mathcal{J}^{\pm}_{\mathrm{bulk}}$ and $\mathcal{J}^{\pm}_{\mathrm{sur}}$ will be zero when the electric field $\boldsymbol{\xi}$ is directed along the armchair direction. These transverse

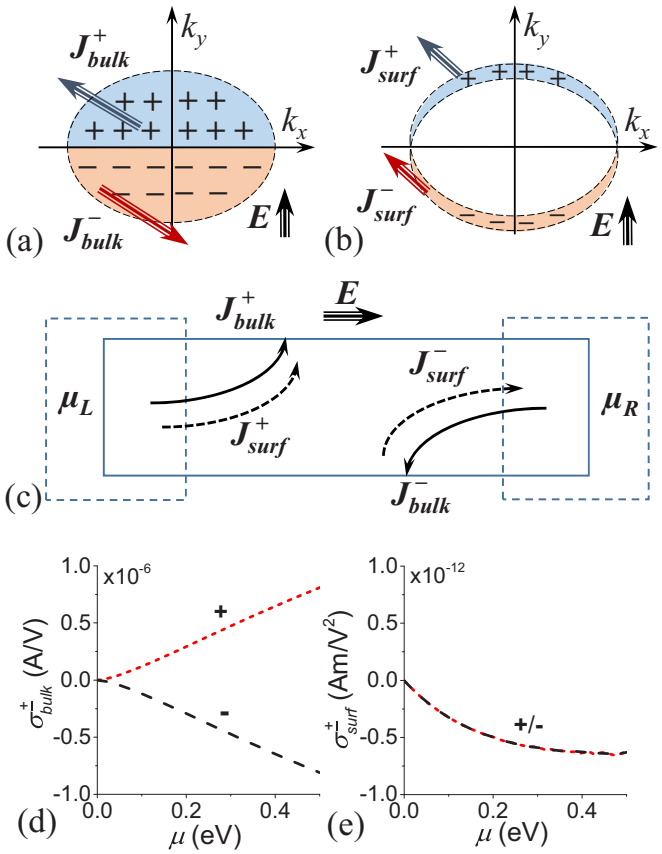

FIG. 2. (Color online) (a) "Bulk Fermi sea" contribution to the transverse current, which can be partitioned into forward/backward propagating currents $\mathcal{J}^{\pm}_{\rm bulk}$. These currents are linear with electric field ξ and persist even in equilibrium. (b) The "Fermi-surface" contribution, also partitioned into $\mathcal{J}^{\pm}_{\rm sur}$, has a ξ^2 dependence and is a nonequilibrium phenomenon. (c) Illustration of the various transverse currents in a typical two terminal device. (d) and (e) Dependence of the bulk and surface transverse currents with Fermi level μ, expressed in terms of their conductivities (see text). Calculations assumed a temperature of 10 K.

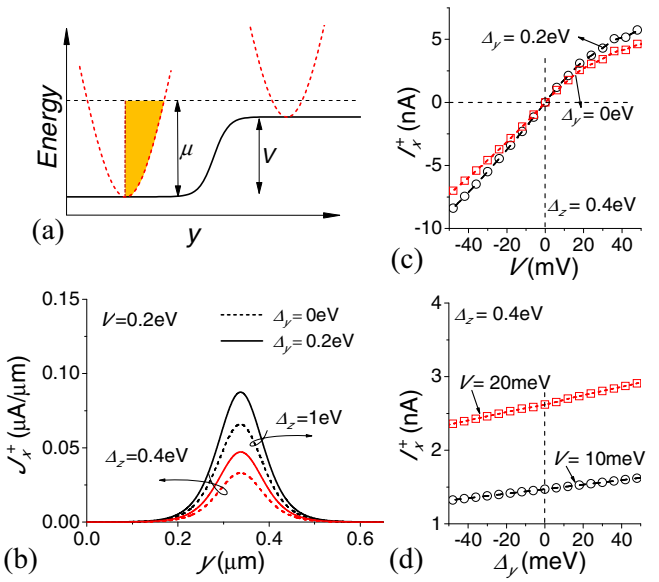

FIG. 3. (Color online) (a) Schematic illustrating the electrostatic junction at equilibrium, along the zigzag y direction. Fermi energy μ and built-in potential V are indicated. (b) Distribution of transverse current density $\mathcal{J}^{+}_{x}(y)$, flowing along x, plotted across the junction, under different applied out-of-plane potential Δ_z and crystal potential Δ_y as indicated (see text). (c) and (d) Integrated transverse current under different applied V and Δ_y, respectively. All calculations assumed $\mu = 0.5$ eV and zero temperature.

currents attain their maximum when $\boldsymbol{\xi}$ is directed along the zigzag direction.

Figures 2(d) and 2(e) plot the dependence of these bulk and surface transverse currents with Fermi level μ, expressed in terms of their conductivities. In a 2D electron gas, $\mu \propto n$, n being the carrier density. We found that $\sigma_{\rm bulk} \propto \mu$ and $\sigma_{\rm surf} \propto \sqrt{\mu}$. This is consistent with the fact that the number of bulk and surface Fermi states scales with μ and $\sqrt{\mu}$, respectively. The computed linear response is an order of magnitude smaller than that predicted for transition-metal dichalcogenides [5]. However, the finite nonlinear response in this case can produce a comparable or larger effect at higher driving fields.

To gain deeper insight into the above-mentioned issues, we consider an edge-free model system, an electrostatic junction with a built-in electric field aligned along the zigzag (i.e., y) direction. The electrostatic junction provides a built-in electric field that drives the transverse bulk current response. Here, we consider the device under an equilibrium condition.

Our approach solves the quantum-mechanical scattering problem microscopically within the above-mentioned tight-binding model. We describe this built-in junction with $V(y) = V\tanh(\frac{x}{\alpha})$, as shown in Fig. 3(a), where V is the built-in potential. In this calculation, we assumed a junction transition length of $\alpha = 60$ nm. The Fermi energy, μ, is biased within the lowest conduction band of BP. We consider the combined effect of an out-of-plane electric field, $V_1 = V_2 = \frac{1}{2}\Delta_z$ and $V_3 = V_4 = -\frac{1}{2}\Delta_z$, and a periodic crystal potential commensurate with the BP unit cell, $V_1 = V_4 = \frac{1}{2}\Delta_y$ and $V_2 = V_3 = -\frac{1}{2}\Delta_y$. A periodic boundary condition is imposed along x, hence k_x can be regarded as a good quantum number. Assuming semi-infinite perfect leads, then what we have is essentially a one-dimensional quantum scattering problem. The scattering wave functions of the tight-binding problem, as well as a key local observable (e.g., current density, the quantity of interest here), can be solved numerically through standard approaches [15–17]. In the following, we show that a transverse current can indeed flow along the junction, i.e., x direction, when appropriate symmetries are broken in consistence with the semiclassical discussion above.

We are interested in the transverse current arising from the forward propagating states deep in the Fermi sea, as depicted by the shaded part of the energy dispersion in Fig. 3(a). Here, all calculations assumed $\mu = 0.5$ eV and zero temperature. In Fig. 3(b), we plot the calculated transverse current density profile $\mathcal{J}^{+}_{x}(y)$ across the junction, assuming $V = 0.2$ eV. When Δ_y and Δ_z are nonzero, crystalline inversion symmetry is broken and a finite Berry curvature is present. Indeed, a finite transverse current can be observed, which peaks at the middle of the junction where the electric field is maximum. Away from the junction, $\mathcal{J}^{+}_{x}$ goes to zero.

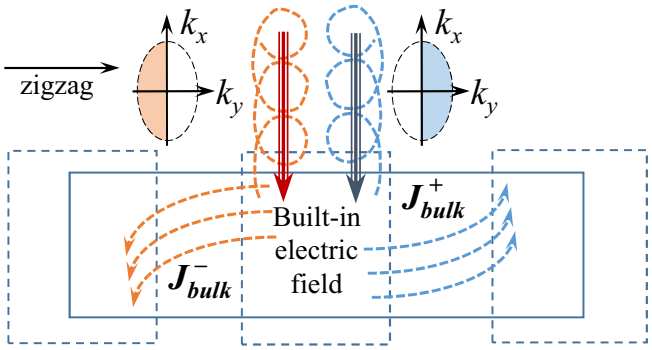

FIG. 4. (Color online) Schematic illustrating the excitation of states with positive or negative Berry curvatures with circularly polarized light. For example, right circularly polarized light couples to states with positive Berry curvatures, which will produce an electrical current flowing towards the right contact and the top edge. The transversal current changes sign with Δ_z.

Symmetry arguments inform us that the transverse current should be odd with respect to V, i.e., $\mathcal{J}_x^{\pm}(-V) = -\mathcal{J}_x^{\pm}(V)$. In the small V limit, the Hamiltonian will recover the mirror symmetry $\mathcal{M}_y$. Since $\mathcal{M}_y$ does not affect the transverse current, we have $\mathcal{J}_x^{+}(-V) = \mathcal{J}_x^{-}(V)$. On the other hand, time-reversal symmetry would require $\mathcal{J}_x^{+}(V) = -\mathcal{J}_x^{-}(V)$. Taken together, we have $\mathcal{J}_x^{+}(-V) = -\mathcal{J}_x^{+}(V)$. Hence, the response to a small applied V should be linear. Numerical results shown in Fig. 3(c) confirm this simple argument.

From the numerics, we found that the transverse current has two distinct contributions, i.e., $\mathcal{I}_x^{+} \sim \Delta_z\xi + \Delta_y\Delta_z\xi$. These trends can be observed in Figs. 3(c) and 3(d). The latter contribution is analogous to the bulk Fermi sea semiclassical $\mathcal{J}_{\text{bulk}}$ we discussed earlier [18]. At small V, we clearly distinguish the linear regime consistent with the semiclassical result $\mathcal{J}_{\text{bulk}} \propto \xi$. We observed a rollover in $\mathcal{I}_x^{+}$ at larger positive V, as more states deep in the Fermi sea are completely reflected due to the energy barrier. When V is negative, there is no energy barrier, hence the linear trend persists. The former contribution to $\mathcal{I}_x^{+}$ is a residual transverse current that probably has a different origin. A finite Δ_z breaks $\mathcal{M}_x$ symmetry and produces a current along x. Since the magnitude of $\mathcal{I}_x^{+}$ is tunable by varying Δ_z, it provides an obvious way for the detection of the proposed effect. The proposed effect can also be detected optoelectronically. Figure 4 illustrates a possible experimental scheme. Circularly polarized light can couple preferentially to states with Berry curvatures of a particular sign [5,6] and produce a net longitudinal and transversal charge current. We stress that there will be no net charge current in monolayer transition-metal dichalcogenides instead [5], due to cancellation from the two valleys.

Last but not least, we discuss some considerations on the experimental observation of this effect. Breaking of the crystal inversion symmetry is key. Finding the appropriate substrate which is commensurate along the zigzag direction of BP is needed to provide a finite Δ_y. Certainly, high mobility samples are desirable for the observation of the proposed effect. Recently, encapsulation of BP with hexagonal boron nitride [19], all within a controlled inert atmosphere, has allowed for higher carrier mobilities [19–23]. Indeed, high-quality BP has made possible the first observation of prominent quantum magneto-oscillations in these devices [19–23]. The results we obtained here are also applicable to other emerging 2D materials with broken inversion symmetry and anisotropic bands at the Γ valley [24,25].

T.L. and Y.J. acknowledge support from the University of Minnesota startup fund. F.G. acknowledges support from the Spanish Ministry of Economy through Grant No. FIS2011-23713, the European Research Council Advanced Grant (Contract No. 290846), and the European Commission under the Graphene Flagship (Contract No. CNECTICT-604391).

[1] M. V. Berry, Proc. R. Soc. A **392**, 45 (1984).
[2] D. Xiao, M.-C. Chang, and Q. Niu, Rev. Mod. Phys. **82**, 1959 (2010).
[3] N. Nagaosa, J. Sinova, S. Onoda, A. MacDonald, and N. Ong, Rev. Mod. Phys. **82**, 1539 (2010).
[4] M. Z. Hasan and C. L. Kane, Rev. Mod. Phys. **82**, 3045 (2010).
[5] D. Xiao, G.-B. Liu, W. Feng, X. Xu, and W. Yao, Phys. Rev. Lett. **108**, 196802 (2012).
[6] K. F. Mak, K. L. McGill, J. Park, and P. L. McEuen, Science **344**, 1489 (2014).
[7] Y. D. Lensky, J. C. W. Song, P. Samutpraphoot, and L. S. Levitov, Phys. Rev. Lett. **114**, 256601 (2015).
[8] R. Gorbachev, J. Song, G. Yu, A. Kretinin, F. Withers, Y. Cao, A. Mishchenko, I. Grigorieva, K. Novoselov, L. Levitov *et al.*, Science **346**, 448 (2014).
[9] M. Sui, G. Chen, L. Ma, W. Shan, D. Tian, K. Watanabe, T. Taniguchi, X. Jin, W. Yao, D. Xiao *et al.*, arXiv:1501.04685 (2015).
[10] A. Morita, Appl. Phys. A **39**, 227 (1986).
[11] L. Li, Y. Yu, G. J. Ye, Q. Ge, X. Ou, H. Wu, D. Feng, X. H. Chen, and Y. Zhang, Nat. Nanotechnol. **9**, 372 (2014).
[12] H. Liu, A. T. Neal, Z. Zhu, Z. Luo, X. Xu, D. Tománek, and P. D. Ye, ACS Nano **8**, 4033 (2014).
[13] A. N. Rudenko and M. I. Katsnelson, Phys. Rev. B **89**, 201408 (2014).
[14] H. Yu, Y. Wu, G.-B. Liu, X. Xu, and W. Yao, Phys. Rev. Lett. **113**, 156603 (2014).
[15] M. Di Ventra, *Electrical Transport in Nanoscale Systems* (Cambridge University, Cambridge, England, 2008), Vol. 14.
[16] S. Datta, *Electronic Transport in Mesoscopic Systems* (Cambridge University, Cambridge, England, 1997).
[17] J. Tworzydło, B. Trauzettel, M. Titov, A. Rycerz, and C. W. J. Beenakker, Phys. Rev. Lett. **96**, 246802 (2006).
[18] It is worth noting that Δ_z suffices to induce transverse currents. This term breaks geometrical spatial inversion, but not the effective inversion symmetry of the Hamiltonian discussed in the text.
[19] Y. Cao, A. Mishchenko, G. Yu, K. Khestanova, A. Rooney, E. Prestat, A. Kretinin, P. Blake, M. Shalom, G. Balakrishnan *et al.*, Nano Lett. **15**, 4914 (2015).

[20] X. Chen, Y. Wu, Z. Wu, S. Xu, L. Wang, Y. Han, W. Ye, T. Han, Y. He, Y. Cai *et al.*, Nat. Commun. **6**, 7315 (2015).

[21] N. Gillgren, D. Wickramaratne, Y. Shi, T. Espiritu, J. Yang, J. Hu, J. Wei, X. Liu, Z. Mao, K. Watanabe *et al.*, 2D Mater. **2**, 011001 (2015).

[22] L. Li, G. J. Ye, V. Tran, R. Fei, G. Chen, H. Wang, J. Wang, K. Watanabe, T. Taniguchi, L. Yang *et al.*, Nat. Nanotechnol. **10**, 608 (2015).

[23] V. Tayari, N. Hemsworth, I. Fakih, A. Favron, E. Gaufrès, G. Gervais, R. Martel, and T. Szkopek, Nat. Commun. **6**, 7702 (2015).

[24] S. Tongay, H. Sahin, C. Ko, A. Luce, W. Fan, K. Liu, J. Zhou, Y.-S. Huang, C.-H. Ho, J. Yan *et al.*, Nat. Commun. **5**, 3252 (2014).

[25] J. O. Island, M. Barawi, R. Biele, A. Almazán, J. M. Clamagirand, J. R. Ares, C. Sánchez, H. S. van der Zant, J. V. Álvarez, R. D'Agosta *et al.*, Adv. Mater. **27**, 2595 (2015).